# Statistics of surface gravity wave turbulence in the space and time domains.

Sergey Nazarenko,[1] Sergei Lukaschuk,[2] Stuart McLelland,[3] and Petr Denissenko[4]

[1]*Mathematics Institute, Warwick University, Coventry, CV4 7AL, UK*

[2]*Department of Engineering Hull University, Hull, HU6 7RX, UK**

[3]*Department of Geography, Hull University, Hull, HU6 7RX, UK*

[4]*School of Engineering, Warwick University, Coventry, CV4 7AL, UK*

(Dated: November 16, 2008)

## Abstract

We present experimental results on simultaneous space-time measurements for the gravity wave turbulence in a large laboratory flume. We compare these results with predictions of the weak turbulence theory (WTT) based on random waves, as well as with predictions based on the coherent singular wave crests. We see that both wavenumber and the frequency spectra are not universal and dependent on the wave strength, with some evidence in favor of WTT at larger wave intensities when the finite flume effects are minimal. We present further theoretical analysis of the role of the random and coherent waves in the wave probability density function (PDF) and the structure functions (SFs). Analyzing our experimental data we found that the random waves and the coherent structures/breaks coexist: the former show themselves in a quasi-gaussian PDF core and in the low-order SFs, and the latter - in the PDF tails and the high-order SF's. It appears that the $x$-space signal is more intermittent than the $t$-space signal, and the $x$-space SFs capture more singular coherent structures than do the $t$-space SFs. We outline an approach treating the interactions of these random and coherent components as a turbulence cycle characterized by the turbulence fluxes in both the wavenumber and the amplitude spaces.

PACS numbers: 47.35.Bb, 47.35.Jk, 47.54.De, 47.35.-i

*Also at The Institute of Automation and Electrometry, SBRAS, Novosibirsk; Electronic address: S.Lukaschuk@hull.ac.uk

## I. INTRODUCTION

Understanding statistics of random water surface waves and their mutual nonlinear interactions mechanisms is important for the wave forecasting, weather and climate modeling [1]. Field observations of the sea surface, laboratory experiments in wave flumes and numerical simulations are efficient and complimentary tools for studying such random nonlinear waves and for testing existing theoretical models. Obvious advantage of the field observations is that they deal directly with the system we want to know about, rather than model it in a scaled-down laboratory experiment or in numerical simulation. In comparison with field measurements, laboratory experiments and numerical simulations allow more control over the physical conditions and over the quantities we measure, especially in the numerical simulations which allows us to access a much broader range of diagnostics than in experiments.

On the other hand, the laboratory experiments enable observations of much larger range of wave scales than it is possible in numerical simulations under the current level of resolution and, therefore, they allow to obtain cleaner power-law spectra and other scalings. Furthermore, laboratory experiments are much more realistic than numerics in reproducing the strongly nonlinear events because most numerical methods are based on weakly nonlinear truncations of the original fluid equations. Finally, they also have a natural dissipation mechanism as in open seas, wave breaking, in contrast to an artificial hyper-viscous dissipation which is usually used in numerics.

In the present paper, we report on new experimental results in a laboratory flume of dimensions 12m x 6m x 1.5m. In our previous experiments at this facility [2] we measured time series of the surface elevation at several fixed locations on the two-dimensional plane using point-like wire capacitance probes. This is a standard technique which was also used in smaller experiments [3], and which allows one to obtain the wave spectra in the frequency domain, as well as higher order statistics of the surface heights from the time series acquired at fixed spatial locations. For weakly nonlinear waves, such measurements seem to be sufficient for obtaining information about the space distributions of the waves (e.g. the wavenumber spectra) via the linear wave dispersion relation $\omega = \sqrt{gk}$. On the other hand, our previous experimental results [2] indicated that in the laboratory flumes there are significant finite-size effects which can be overcome only at rather high levels of nonlinearity of the wave field. In particular, at high averaged wave field intensities we observed a better agreement with

the $\omega^{-4}$ prediction of the Zakharov-Filonenko (ZF) [4, 5] wave turbulence theory developed for weakly nonlinear waves with almost random phases. On the other hand, the same $\omega^{-4}$ spectrum was predicted by Kuznetsov (Ku) [6] based on the assumption that the dominant contribution to the power-law scaling comes from sharp wave-crests with one-dimensional ridges whose velocity remains nearly constant while crossing the wire probe. Obviously, the nonlinearity of such wave-crests is high and one cannot use the linear dispersion relation for obtaining the space statistics out of the time statistics. This situation demonstrates that the frequency spectrum alone does not allow us to distinguish between such drastically different types of waves: random phased modes and sharp-crested structures. On the other hand, ZF and Ku theories predict very different shape of the $k$-spectra, $k^{-2.5}$ (for one dimensional, 1D, spectral density) vs $k^{-4}$ respectively. Thus, a direct method of measuring $k$-spectra could allow one to differentiate between the ZF and Ku states.

Besides, even for rather weakly nonlinear on average fields, occasional strongly nonlinear wave-crests and wave-breaks are known to occur. In spite of being seldom, these structures are crucial because they provide the main mechanism for dissipation of the wave energy, and they are related to the phenomenon of intermittency of wave turbulence. Again, since such seldom events are strongly nonlinear, one cannot use the linear dispersion relation for understanding their statistics, and a direct $x$-space measurement is desirable.

With these motivations in mind, in the present work we have implemented a new technique for direct one dimensional measuring of instantaneous surface profiles (see details below). Thus, we are able to measure the $k$-spectra directly, as well as the higher order $x$-space statistics averaged over a discrete set of instants of time, particularly PDFs and SFs of the height increments in space. This can be done at different levels of wave forcing, but we have excluded the range of very weak forcing for which the finite flume size effects were shown to be significant. This was primarily to achieve better scaling regimes since at low intensities the spectra are very steep and span over smaller ranges of scales with some peaks often obscuring the power-law fits [2]. The $x$-space measurements are accompanied by the capacitance fixed point measurements of the $t$-series for the same experimental runs, which gives us simultaneous information about the space and time domain statistics of the water surface elevation.

The main message of the present paper is that the wave turbulence behavior is typically non-universal and reflects presence of two coexisting species: weak incoherent waves and

sparse but strong sharp wave-crest structures. The incoherent waves dominate in the spectra and the scalings of the low order structure functions. These scaling agree with ZF weak turbulence predictions for the spectra at higher amplitudes. Moreover, we see consistency with ZF scalings for the low-order SFs at relatively high amplitudes (when the finite size effects are minimal). Further, ZF theory appears to agree better with the $t$-domain than for the $\omega$-domain statistics, which is clearly the finite inertial range effect (because the $t$- and the $\omega$-objects are related via the Fourier transform). For the higher order SFs, we see behavior characteristic of intermittency and presence of singular coherent structures. Interestingly, propagating Ku-type 1D wave crests are better detected by the $t$-space SFs, and the $x$-space SFs capture more singular almost non-propagating wave crests schematically shown in Figure 2.

Our paper is organized as follows. In Section two we describe the relevant theories and predictions for the surface wave turbulence. In Section three we describe the experimental facility and the measurement techniques. In Section four we present the experimental results along with their discussion in the context of the theoretical predictions and possible interpretations. In Section five we present a summary of our findings and an outlook for a future work.

## II. THEORETICAL BACKGROUND.

Let us start with a theoretical background including an overview of the existing theoretical predictions as well as a further analysis of the statistical objects relevant to our experiments.

### A. Spectra.

First, let us define the wave energy spectrum in the frequency domain as

$$E_\omega = \int e^{i\omega t'} \langle \eta(\mathbf{x}, t)\eta(\mathbf{x}, t + t')\rangle \, dt', \tag{1}$$

and the 1D energy spectrum in the wavenumber domain, respectively, as

$$E_k = \int e^{ikz} \langle \eta(\mathbf{x}, t)\eta(\mathbf{x} + \mathbf{w}z, t)\rangle \, dz, \tag{2}$$

where $\eta(\mathbf{x}, t)$ is the surface elevation at time $t$ and location in the horizontal plane $\mathbf{x} = (x, y)$. The integration in (1) is taken over a time window, and in (2) - over a piece of straight line

in the 2D plane illuminated by the laser sheet (with $\mathbf{w}$ being a unit vector along this line). angle brackets mean ensemble averaging over realizations (equivalent to the time averaging in presence of ergodicity). For a statistically steady and homogeneous state, $E_\omega$ and $E_k$ are independent of $t$ and $\mathbf{x}$. Most of the theories predict a power-law scaling

$$E_\omega \propto \omega^{-\nu} \tag{3}$$

and

$$E_k \propto k^{-\mu} \tag{4}$$

where the indices $\nu$ and $\mu$ depend on a particular theory.

### B. Statistics of the field increments.

The spectra considered in the previous section correspond to the second-order correlators. Different types of coherent and incoherent structures may lead to the same spectra. One, therefore, must consider higher-order correlators to see an unequivocal signature of a particular kind of coherent structures or incoherent random phased field.

To study the higher-order statistics in our previous paper [2] we considered PDFs of the wave crest heights, as well as PDFs of a band-pass filtered field (the theory for the later was developed in [7]). Here, we will also consider other (very popular in turbulence theory) objects: space and time elevation field increments of different orders which are defined as follows,

$$\delta_l^{(1)} = \eta(\mathbf{x}+\mathbf{l}) - \eta(\mathbf{x}), \tag{5}$$

$$\delta_l^{(2)} = \eta(\mathbf{x}+\mathbf{l}) - 2\eta(\mathbf{x}) + \eta(\mathbf{x}-\mathbf{l}), \tag{6}$$

etc. (here all $\eta$'s are taken at the same $t$), and

$$\delta_\tau^{(1)} = \eta(t+\tau) - \eta(t), \tag{7}$$

$$\delta_\tau^{(2)} = \eta(t+\tau) - 2\eta(t) + \eta(t-\tau), \tag{8}$$

etc. (here all $\eta$'s are taken at the same $x$).

*1. Probability density functions.*

PDFs of the above increments $P_x(\sigma)$ and $P_t(\sigma)$ are defined in the usual way as a probability of a particular increment to be in the range from $\sigma$ to $\sigma + d\sigma$ divided by $d\sigma$, or in the symbolic form

$$P_x^{(j)}(\sigma) = \langle \delta(\sigma - \delta_l^{(j)}) \rangle, \tag{9}$$

and

$$P_t^{(j)}(\sigma) = \langle \delta(\sigma - \delta_\tau^{(j)}) \rangle \tag{10}$$

respectively, where $j = 1, 2, \ldots$. For random phased fields, these PDFs are Gaussian, and presence of sparse coherent structures can be detected by the deviations from Gaussianity at the PDF tails. In particular, fatter than Gaussian tails indicate an enhanced probability of strong bursts in the signal which is called intermittency.

*2. Structure functions.*

Let us now introduce the moments of the height increments, which are called the *structure functions*,

$$S_l^{(j)}(p) = \langle (\delta_l^{(j)})^p \rangle = \int \sigma^p P_x^{(j)}(\sigma)\, d\sigma, \tag{11}$$

and

$$S_\tau^{(j)}(p) = \langle (\delta_\tau^{(j)})^p \rangle = \int \sigma^p P_t^{(j)}(\sigma)\, d\sigma. \tag{12}$$

Often in turbulence, the structure functions asymptotically tend to scaling laws,

$$S_l^{(j)}(p) \sim l^{\xi(p)} \tag{13}$$

in the limit $l \to 0$, and

$$S_\tau^{(j)}(p) \sim \tau^{\zeta(p)} \tag{14}$$

in the limit $\tau \to 0$ respectively. Functions $\xi(p)$ and $\zeta(p)$ are called the SF scaling exponents, and they contain the most important information about the turbulent field coherent and incoherent components and, correspondingly, about the turbulence intermittency.

### C. Scalings generated by random phased waves.

*1. Spectra.*

Weak turbulence theory (WTT) considers weakly nonlinear random-phased waves in an infinite box limit. For the wave spectrum, these assumptions lead to the so-called Hasselmann equation [8]. This equation is quite lengthy and for our purposes it suffices to say that the ZF energy spectrum

$$E_\omega \propto \omega^{-4} \tag{15}$$

is an exact solution of Hasselmann equation which describes a steady state with energy cascading through an inertial range of scales from large scales, where it is produced, to the small scales where it is dissipated by wavebreaking. In the $k$-domain, the one-dimensional ZF energy spectrum is

$$E_k \propto k^{-5/2}. \tag{16}$$

It is important that in deriving WTT, the limit of an infinite box is taken before the limit of small nonlinearity. This means that in a however large but finite box, the wave intensity should be strong enough so that the nonlinear resonance broadening is much greater than the spacing of the $k$-grid (corresponding to Fourier modes in a finite rectangular box). As estimated in [9], this implies a condition on the minimal angle of the surface elevation $\gamma > 1/(kL)^{1/4}$, where $L$ is the size of the basin, which is quite a severe restriction. If this condition is not satisfied the number of exact and quasi four-wave resonances will be drastically depleted [9, 10, 11]. This can lead to a significant slowdown of the energy cascade from long to short waves and, therefore, a steeper energy spectrum. A theory of discrete wave turbulence developed in [9] for very low levels of forcing predicts $E_\omega \propto \omega^{-6}$, which is confirmed in experiments with very weak forcing [2]. On the other hand, for such weak forcing the scaling interval is rather short and not very well formed (it contains some peaks). Thus, in the present paper we will deal with stronger wave fields for which the spectra are shallower ($\nu \lesssim 5.5$), even though it is still steeper than ZF due to the finite-size effects.

*2. PDF and the structure functions.*

Now let us consider a wave field made out of modes with random phases and the energy spectrum $E_k \sim k^{-\mu}$. As we mentioned, for random phased fields, the PDFs of the height increments are Gaussian. For Gaussian statistics we immediately have

$$S_l^{(j)}(p) \sim l^{p(\mu-1)/2} \tag{17}$$

if $\mu < 2j+1$, otherwise $S_l^{(j)}(p) \sim l^{pj}$ because the field is $j$ times differentiable.

Similarly, in the time domain we have for the random-phased field with the energy spectrum $E_\omega \sim \omega^{-\nu}$:

$$S_\tau^{(j)}(p) \sim \tau^{p(\nu-1)/2} \tag{18}$$

if $\nu < 2j+1$, otherwise $S_\tau^{(j)}(p) \sim \tau^{pj}$.

### D. Scalings generated by singular coherent structures.

*1. Spectra.*

Sharp wave crests are quite common for gravity waves of sufficiently large amplitudes. The most common type of crests discussed in the literature looks like a break in the surface slope. A prototype for such structures is a sharp-crested stationary Stokes wave solution with the crest angle of 120°. Following Kadomtsev [12], such sharp crested waves are usually associated with the Phillips (Ph) spectrum. Indeed, assume that there are discontinuities occurring at isolated points. This leads to the following one-dimensional energy spectrum in wavenumber space $E_k \propto k^{-3}$. Second, assuming that transition from the $k$-space to the $\omega$-space should be done according to the linear wave relation $\omega = \sqrt{gk}$, we arrive at the Ph spectrum [13],

$$E_\omega = g^2 \omega^{-5}. \tag{19}$$

An alternative way to derive the Ph spectrum, the way it was originally done by Phillips [13], is to assume that the gravity constant $g$ is the only relevant dimensional physical quantity. This argument is equivalent to saying that the linear term is of the same order as the nonlinear one in the water surface equations in the Fourier space.

Kuznetsov [6] questioned this picture and argued that (i) slope breaks occur on one-dimensional lines/ridges rather than on zero-dimensional point/peaks, and (ii) that the

wave-crest is propagating with preserved shape, i.e. $\omega \propto k$ should be used instead of the linear wave relation $\omega = \sqrt{gk}$. This assumptions give $E_\omega \propto \omega^{-4}$, i.e. formally the same scaling as ZF, even though the physics behind it is completely different. Finally, it was proposed in [14] that wave crest ridges may have non-integer fractal dimension $D$ somewhere in the range $0 < D < 2$. This leads to the following one-dimensional energy spectrum in the $k$-space,

$$E_k \propto k^{-3-D}. \tag{20}$$

Assuming, following Kuznetsov, $\omega \propto k$, we have in this case

$$E_\omega \propto \omega^{D-6}. \tag{21}$$

*2. PDF and the structure functions.*

Let us ask what shape of PDF would be produced by structures of Kuznetsov (Ku) type with unit slopes on the both sides and $D = 1$. Let us assume that the position and orientation of such ridges are random in the 2D plane. In this case for $j \geq 2$, a space height increment will have non-zero values only if it has its argument points on both sides of the coherent structure. Let us restrict ourselves to the case $j = 2$; then

$$\begin{aligned} \delta_l^{(2)} &= 2\cos\theta\ (l - z), \quad \text{for } |z| < l, \\ \delta_l^{(2)} &= 0, \qquad\qquad\quad \text{for } |z| > l, \end{aligned} \tag{22}$$

where $l = |\mathbf{l}|$, vector $\mathbf{l}$ is parallel to the axis $x$, $\theta$ is the angle between the normal vector to the coherent structure's ridge and vector $\mathbf{l}$, and $z$ is the distance from the increment middle point and the intersection between the ridge and the line connecting the increment points, see Fig. 1.

For the PDF we have

$$P_x^{(2)}(\sigma) = 0, \quad \text{for } |\sigma| > 2l \tag{23}$$

(the maximal value of the increment is limited by the strength of the singularity), and

$$\begin{aligned} &P_x^{(2)}(\sigma) = \langle \delta(\sigma - \delta_l^{(2)}) \rangle = \\ &\frac{1}{\pi} \int_{-\pi/2}^{\pi/2} d\theta\ \frac{1}{2l} \int_{-l}^{l} dz \quad \delta(\sigma - 2\cos\theta\ (l - z)) = \\ &\frac{1}{2\pi l} \int_0^{\arccos \frac{|\sigma|}{2l}} \frac{d\theta}{\cos\theta} = \frac{1}{2\pi l} \ln \left[ \frac{2l}{|\sigma|} + \sqrt{\left[\frac{2l}{|\sigma|}\right]^2 - 1} \right] \end{aligned} \tag{24}$$

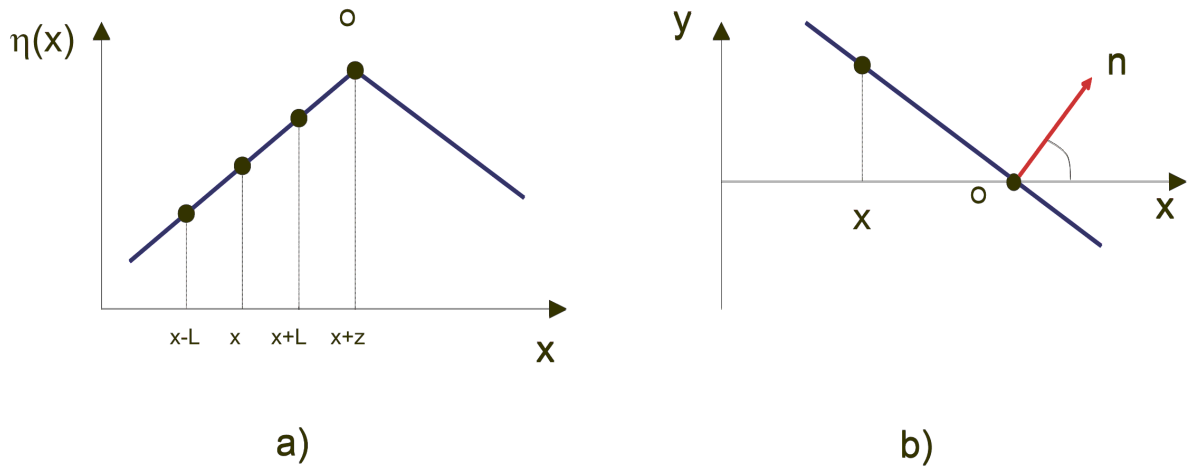


FIG. 1: Schematic of the ridge (coherent structure) cross section used in PDF calculations: a) the Ku-type ridge in the plane $(x, \eta(x))$, where $x$ is directed along the illuminated line on the air-water interface and is parallel to the vector $\mathbf{l}$; b) the same ridge in the $(x, y)$-plane.

for $|\sigma| \leq 2l$.

In the above, we considered a simplified configuration of ridges such that on average only one ridge with slope equal to $\pm 1$ crosses a unit area. This result can be easily extended to the structures with a distribution of the slope values and with an arbitrary density in 2D space. This would move the PDF cutoff to $|\sigma| = 2ls$, where $s$ is the maximal allowed slope of the coherent structures. (Such a PDF cutoff feature was discussed in [7]; see also discussion below in the next subsection). Asymptotic behavior for such general PDF for $|\sigma| \ll 2l$ is

$$P_x^{(2)}(\sigma) \sim \frac{A}{l}\left[\ln\left(\frac{l}{|\sigma|}\right) + B\right], \tag{25}$$

where $A$ and $B$ are dimensionless constants which depend on the strength distribution of the singular ridges and their spatial density.

Let us now consider a somewhat more general class of singular coherent structures whose cross-section near the singularity is given by formula

$$\eta(x) = \eta_0 - C_a |x|^a, \tag{26}$$

with a singularity degree constant $a$ such that $0 < a \leq 1$, and constants $\eta_0$ and $C_a$ describing a reference surface elevation and the coherent structure amplitude respectively, see Fig.2. For the simplified structures considered above $a = 1$ and $C_a \approx 1$ which was implied by both

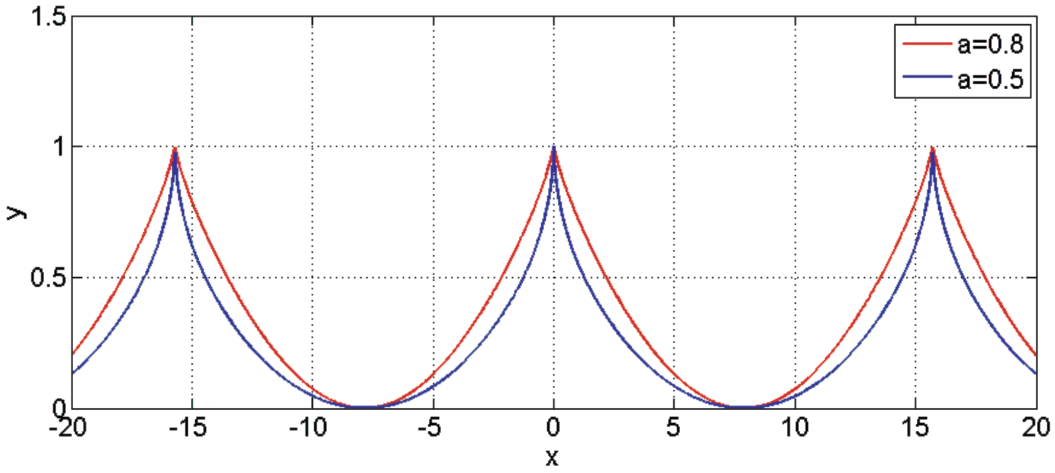


FIG. 2: A wave profile with singular structures of type $\eta(x) = \eta_0 - C_a\,|x|^a$ with $0 < a < 1$. (Plot shows $y = 1 - |\sin(0.2x)|^a$.)

the Ph and Ku models. We will see below that structures with the additional parameter $a < 1$ also seem to be relevant to the wave turbulence in our experiments. For generalization we will assume that the ridges of such crests have a fractal dimension $0 \leq D < 2$ (e.g. 0 for Ph and 1 for Ku).

Contribution to the PDF of the structures with $a < 1$ can be considered as above, and it is easy to see that the corresponding integral of type as in the Eq.24 is convergent. This means that the structures with $a < 1$ contribute to the PDF tails "locally", i.e. structures with amplitudes $C_a$ form a "bump" on the tail near $\sigma = C_a l^a$. The shape of such a bump is not universal and it depends on the distribution of the crests over $C_a$.

On the other hand, an effective way to detect the structures is to consider the SFs and their scalings in $l$ (note that the PDFs are usually measured at fixed $l$'s and, therefore, the corresponding scalings in $l$ are hard to obtain, e.g. due to insufficient statistical data). We will be interested in the limit $l \to 0$ of the structure functions $S_l^{(j)}(p)$. Suppose that there are $N$ coherent structures per unit area. The probability for having points of the structure function on the two different sides of the coherent structure ridge is $Nl^{2-D}$. The probability to have all the point on the same side of the ridge is $1 - l^{2-D} \approx 1$ (for $l \to 0$). If all the points are on the same side of the ridge then, assuming that away from the ridge the field is $j$ times differentiable, $\delta_l^{(j)} \sim l^j$, whereas if the points are on the different sides of the ridge

$\delta_l^{(j)} \sim l^a$, so

$$S_l^{(j)}(p) \sim l^{pj} + Nl^{2-D+ap}. \tag{27}$$

Note that in the limit $l \to 0$ out of the two terms on the RHS the one with the smallest power will be dominant. Thus, the structures of Ph or Ku type, i.e. with $a = 0$ and $a = 1$, will not bee seen in SFs for the first-order increments and we would have to consider $j \geq 2$. However, one should keep in mind that the finite range of excited scales makes determination of the scalings less precise for higher orders $j$ because of the higher number of SF points to be placed in this finite range. Therefore, it is better to consider the lowest $j$ that could allow to extract the scalings induced by the coherent structures ($j = 2$ in case of the Ph and Ku).

Now suppose that the wave field is bi-fractal and consists of two components: random phased modes and singular coherent structures. Avoiding the choices of $j$ for which the field is $j$ times differentiable, we have in this case

$$S_l^{(j)}(p) \sim l^{p(\mu-1)/2} + l^{2-D+ap}. \tag{28}$$

If $a < (\mu - 1)/2$ we expect to see the scaling associated with the incoherent random phased component at low $p$'s (first term on the RHS) and the singular coherent structure scaling at high $p$'s (second term on the RHS).

Similarly, one can consider the SFs of the time increments. Assuming following Kuznetsov that the coherent structures could be thought as passing the wire probes with constant velocity (due to shortness of the time needed for the singular ridge to pass the probe), we should obtain the time-domain scalings to be identical to the space-domain scalings obtained above, i.e. $S_\tau^{(j)}(p) \sim \tau^{2-D+ap}$.

In the case when incoherent waves and singular coherent structures are present simultaneously, we have

$$S_\tau^{(j)}(p) \sim \tau^{p(\nu-1)/2} + \tau^{2-D+ap}. \tag{29}$$

As before, it is understood here that the order $j$ is chosen in such a way that the field associated with the incoherent wave component is not $j$ times differentiable in time. For example, for spectra with $3 < \nu < 5$ (e.g. for ZF spectrum) one should use $j \geq 2$, and for $5 < \nu < 7$ one should use $j \geq 3$, etc.

### E. Turbulence cycle and fluxes in the wavenumber-amplitude space.

In the previous sections we used the Fourier space for the spectra whereas the higher order statistics was described in terms of the $x$ and $t$-domain increments. In this subsection, we will outline how one can put turbulence containing of incoherent waves and coherent structures onto the same "map". Namely, we will be interested in a turbulence cycle where the structures arise from the turbulent cascade of incoherent waves and, in turn, incoherent waves arise during breaking of the structures. The key element of this picture is combining fluxes over wavenumbers (associated with the Kolmogorov-Zakharov cascade states) and over the wave amplitudes (considered in [7] and linked to intermittency).

Let us summarize the findings of [7], where the WTT formalism was extended to PDF of Fourier intensities $J_k = |a_k|^2$ which is defined as

$$\mathcal{P}_k(J) = \langle \delta(J - |a_k|^2) \rangle. \tag{30}$$

Under the usual WTT assumptions (weak nonlinearity, random phases and amplitudes of the Fourier modes), the following equation for such a PDF was derived,

$$\dot{\mathcal{P}} + \partial_J F = 0, \tag{31}$$

where

$$F = -J(\beta \mathcal{P} + \alpha \partial_J \mathcal{P}) \tag{32}$$

is a probability flux in the $J$-space, and

$$\alpha_k = 4\pi \int |W(\mathbf{k}, \mathbf{k}_1, \mathbf{k}_2, \mathbf{k}_3)|^2 \delta(\mathbf{k} + \mathbf{k}_1 - \mathbf{k}_2 - \mathbf{k}_3) \delta(\omega_k + \omega_{k_1} - \omega_{k_2} - \omega_{k_2}) n_{k_1} n_{k_2} n_{k_3} \, d\mathbf{k_1} d\mathbf{k_2} d\mathbf{k_3},$$

$$\beta_k = 8\pi \int |W(\mathbf{k}, \mathbf{k}_1, \mathbf{k}_2, \mathbf{k}_3)|^2 \delta(\mathbf{k} + \mathbf{k}_1 - \mathbf{k}_2 - \mathbf{k}_3) \delta(\omega_k + \omega_{k_1} - \omega_{k_2} - \omega_{k_2}) \Big[ n_{k_1}(n_{k_2} + n_{k_3}) - n_{k_2} n_{k_3} \Big] \, d\mathbf{k_1} d\mathbf{k_2} d\mathbf{k_3},$$

where $n_k = \langle J \rangle$ and $W(\mathbf{k}, \mathbf{k}_1, \mathbf{k}_2, \mathbf{k}_3)$ is the nonlinearity coefficient which for the case of the surface gravity waves can be found in [19]. It was shown that there are solutions for such wave PDFs that have power-law tails and which, therefore, correspond to the states with turbulent intermittency. These solutions correspond to a constant $J$-flux of probability, $F = \text{const}$. At the tail of the PDF, $J \gg \langle J \rangle = n_k$, the solution can be represented as series in $n_k/J$,

$$\mathcal{P}_k(J) = -F/(J\beta) - \alpha F/(\beta J)^2 + \cdots. \tag{33}$$

It was speculated that such a flux in the amplitude space can be physically generated by the wave breaking events. On the other hand, we know that the ZF state (and, in general, KZ spectra in other applications) corresponds to the energy flux through wavenumbers $k$. Below, we will consider a combined flux which has both $k$ and $J$ components and, thereby, clarify the picture of the wave turbulence cycle which involves both random waves and coherent structures which can get transformed into each other.

First note that the situation is quite subtle because the intermittent solution corresponds to the negative $J$-flux, i.e. from large to small amplitudes, whereas naively one would expect the opposite direction based on the picture that the wave breaking occurs and dissipates turbulence when amplitudes become large. To resolve this "paradox", one should remember that when amplitudes become large the all $k$-modes become correlated (i.e. we observe occurrence of the coherent structures). Namely, these modes are concentrated at the following lines in the $(k, J)$-plane,

$$J_{Ph} \sim g^{1/2} k^{-9/2},$$

see Figure 3. Note that the subscript Ph here stands for "Phillips" to emphasize that it corresponds to the Phillips scaling where the linear and nonlinear terms are of the same order. Let us consider the fluxes on the $(k, J)$-plane. Let us force turbulence by generating weak waves at low $k$'s, - region marked by $\bigoplus$ in Figure 3. The energy cascade will proceed from the forcing region to higher $k$ predominantly along the curve $J(k) = \langle J_k \rangle = n_k$. For example, for the ZF state this curve is

$$J(k) = n_{ZF}(k) \sim \epsilon^{1/3} k^{-4}.$$

Around some scale $k_*$, where the Ph and ZF curves intersect, the WTT description breaks down because the nonlinear term becomes of the same order as the linear one. At this point, the phases get correlated, which arises in the form of coherent structures in the $x$-space. Such coherent structures are made of a broad range of Fourier modes which are correlated and for each of whom the linear and nonlinear terms are in balance. Indeed, if the linear term for some $k$ was greater than the nonlinear term, then this wave would quickly de-correlate from the rest of the modes. If, on the other hand, the nonlinear term gets larger than the linear one at some $k$, then the inertial forces on a fluid element would get larger than the gravity force, and this fluid element would separate from the surface and exit the coherent structure. However, such sea spray and foam do form occasionally via wave breaking which provides the

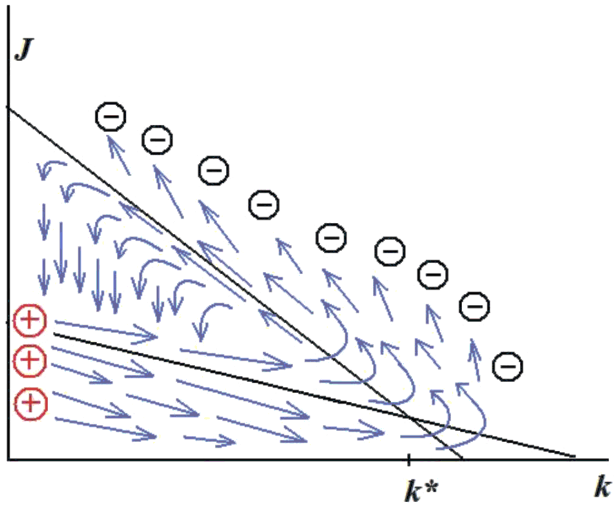


FIG. 3: Turbulent probability fluxes in the $(k, J)$-plane.

main mechanism of the wave energy dissipation. Thus, on the $(k, J)$-plane, the flux turns at $k_*$ and goes back to lower $k$'s along the Ph curve, with some energy lost to the regions above the Ph curve via wave breaking. Occasionally, the coherent structures lose their coherence due to the energy loss to the sea spray and foam and corresponding reduction in nonlinearity. Additional mechanisms that can promote de-correlation of coherent structures and due to their mutual interactions and due to interactions with the incoherent component. On the $(k, J)$-plane, this corresponds to turning of the flux down below the Ph curve and toward the ZF curve. This closes the cycle of the wave turbulence, in which the energy cascade of the random phased waves leads to creation of coherent structures, which in turn, break down with their energy partially dissipated in whitecapping and partially returned into the incoherent random phased component. The exact partition of the energy dissipated vs the energy returned into the random waves is not known, but it is natural to think that these parts are of the same order of magnitude.

The last part of the wave turbulence cycle is crucial for understanding intermittency. Indeed, this part corresponds to a flux in the opposite $J$-direction, which, as we mentioned, corresponds to the power-law tails of the PDF of the Fourier modes.

Note that the wave turbulence cycle picture similar to the one described above was previously suggested in [15] in the context of the inverse cascade in optical wave turbulence

in NLS model with focusing nonlinearity (see also a detailed description in the concluding section of [16] and in a recent paper [17]). In this case, the inverse waveaction cascade proceeds within the incoherent weakly nonlinear wave component until it reaches some (low) wavenumbers where the nonlinearity ceases to be small and the modulational instability sets in. The modulational instability evolves into wave collapses which are strongly nonlinear singular events shrinking to a very small spatial size in finite time. The collapse dissipates part of the waveaction supplied to it via the inverse cascade, whereas the remaining waveaction returns back to the system of random waves because the collapse spike has a significant high-$k$ component which becomes incoherent when after the collapse burn-out.

The qualitative picture of the wave turbulence cycle outlined above can yield to some important qualitative predictions. From the definition of the energy flux in the $k$ space, $\epsilon_k$, and by taking the first moment of equation (31), he have

$$\dot{E}_k = -\partial_k \epsilon_k = 2\pi k\, \omega_k \int_0^{J_{Ph}} J \partial_J F_k \, dJ, \tag{34}$$

where we took into account the relation $E_k = 2\pi k\, \omega_k\, n_k$, and we took into account the cutoff at $J = J_{Ph}$ related to the fact that for $J > J_{Ph}$ the nonlinearity is stronger than the linear terms which means severe damping via wave breaking (i.e. the gravity force is not able to keep the fluid particles attached to the surface). This leads to the following estimate of the relationship between the $J-$ and the $k-$ fluxes,

$$F_k \sim \frac{\partial_k \epsilon_k}{2\pi k\, \omega_k\, J_{Ph}}, \tag{35}$$

Thus, the intermittent tail of the PDF (33) becomes

$$\mathcal{P}_k(J) \approx \frac{F_k}{J\beta_k} \sim \frac{\partial_k \epsilon_k}{2\pi k\, \omega_k\, \beta J\, J_{Ph}} \sim \frac{n_k}{J\, J_{Ph}}. \tag{36}$$

Here, we used the fact that in the kinetic equation

$$\dot{n}_k = \alpha_k - \beta_k n_k \tag{37}$$

the two terms on the RHS are of the same order.

The PDF tail (36) gives the following contribution to the moments of the Fourier amplitudes

$$M_k^{(p),tail} = \int_0^{JPh} J^p\, \mathcal{P}_k(J)\, dJ \sim \frac{n_k}{p}\, J_{Ph}^{(p-1)}. \tag{38}$$

For example, for the ZF states $n_k = n_{ZF}$, we have

$$M_k^{(p),tail} \sim \frac{1}{p}\,\epsilon^{1/3} g^{(p-1)/2}\, k^{1/2-9p/2}. \tag{39}$$

On the other hand, the PDFs core has a Rayleigh shape,

$$\mathcal{P}_k(J) \approx \frac{1}{n_k}\, e^{-J/n_k},$$

which corresponds to Gaussian statistics of the wave field. The core part gives the following contribution to the moments,

$$M_k^{(p),core} = p! n_k^p. \tag{40}$$

For the ratio of the tail and core contributions we have

$$M_k^{(p),tail}/M_k^{(p),core} \sim \frac{1}{pp!}\,\left(J_{Ph}/n_k\right)^{(p-1)}. \tag{41}$$

In particular, for the ZF state

$$M_k^{(p),tail}/M_k^{(p),core} \sim \frac{1}{pp!}\,\left(\frac{k}{k_*}\right)^{(1-p)/2}, \tag{42}$$

where $k_* = g\epsilon^{-2/3}$.

Thus we can see that for a fixed $p > 1$ and at a fixed $k$, the PDF tail will dominate in the moments as $\epsilon \to 0$. On the other hand, at fixed $\epsilon$ and $k$, the core will dominate when $p \to \infty$.

## III. EXPERIMENTAL SETUP.

The experiments were conducted in a rectangular tank with dimensions 12 x 6 x 1.5 meters filled with water up to the depth of 0.9 meters, see Fig. 4. The gravity waves were excited by a piston-type wavemaker. The wavemaker consists of 8 vertical paddles of width 0.75 m covering the full span of one short side of the tank. An amplitude, frequency and phase can be set for each panel independently enabling to control directional distribution of the generated waves. A motion controller is used to program parameters of the generated wave field by specifying its amplitude and a number of wavevectors (given by a set of frequencies and directions). In the experiments described here the wavemaker generated a superposition of two waves of equal amplitude with frequencies $f_1$=0.993Hz and $f_2$=1.14Hz (the wavelength

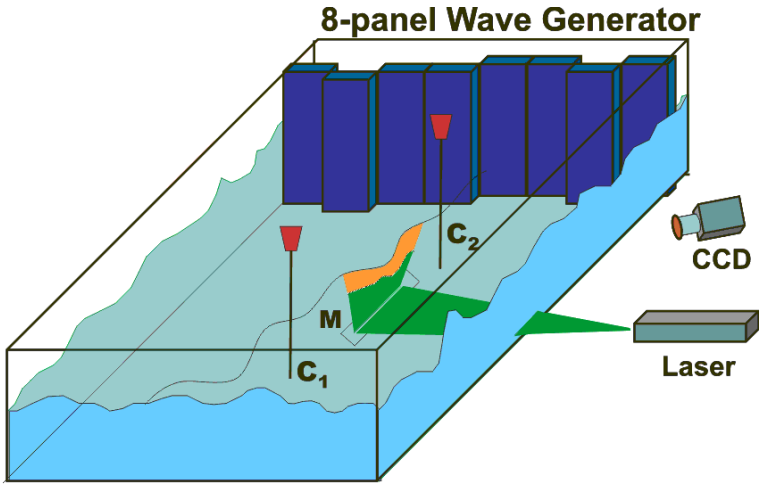


FIG. 4: The experimental setup. M - the first surface mirror, $C_1$ and $C_2$ - the capacitance wire probes, CCD - the digital camera.

is about . The wavevector $k_1$ was perpendicular to the plane of the wavemaker and $k_2$ was at the angle 7° to $k_1$. It is assumed that energy dissipation is low and the waves undergo multiple reflections from the flume walls, interact to each other and form a chaotic wave field homogeneous in the central area of the flume. The main control parameter was an oscillation amplitude of the wavemaker, by varying it we study the dependence of the spectrum and PDFs on the average wave intensity.

Two capacitance wire probes were used to measure the wave elevation as a function of time $\eta(t)$ in two fixed points in the central part of the flume (as it shown in Figure 4). The distance between the probes was 2m. Signals from the probes were amplified and digitized by a 16-bit analog-to-digital converter (NI6035) controlled by the LabView and stored in a PC. Typical signal acquisition parameters were as follows: the bandwidth - 32 Hz and the recording time - 2000 seconds. The wire probes were calibrated before the measurements in the same tank with a stationary water surface.

In addition to measurements of the time dependance, in the present work we introduced a new technique, similar to [18] which allows us to measure the dependence of the surface elevation on the space coordinate along a line. For this we used a vertical cross section image of the air-water interface. The upper layer of water was colored by a fluorescent dye Rhodamine 6G. The water-air interface area was illuminated from below by a narrow light sheet from a pulsed Yag laser (power 120 mW, wavelength 532 nm), see Figure 4. The

images were captured by a 1.3 Mpixel digital camera (Basler, A622f) synchronously with laser pulses at the sampling frequency 8 Hz. The image size is 900 x 1200 mm with the resolution 0.93 mm/pixel and 0.90 mm/pixel in the vertical and the horizontal directions respectively. Typically, we collected five sets of images, each set consisting of 240 frames. The time interval between the sets was 5 minutes. The data from the capacitance probes were acquired continuously and in parallel with the images during this time. The measurements were done at fixed excitation parameters. The measurement procedure included setting the amplitude of the wavemaker oscillations, waiting for a transient time interval, 20-30 min, and recording the signals during 35 min.

The data were processed using the Matlab. The wire probe data were filtered by a band-pass filter within 0.01-20Hz frequency band. The image sets were processed using standard binarization and the boundary detection procedures from the Image Processing Toolbox. Detected air-water boundaries were stored as a set of boundary arrays $\eta(x)$ for a following statistical analysis. The images where the boundary was not a single valued function of $x$ or when it had significant jumps ($|\delta\eta(x)|/\delta x| > 4$) were deleted. A proportion of such images was less than 3%. To calculate spectra from wire probes we used the Welch algorithm with the Hamming window and the averaging performed over 1000 spectral estimates for each signal record. The $k-$spectra were calculated for each array of boundaries (one array from each image) and then averaged over a set from up to 1200 images for each stationary wave field.

As a characteristics of the averaged wave amplitude we used a nonlinearity parameter which is defined as the mean slope of the wave at the energy containing scale, $\gamma = k_m A$, where $k_m$ is the wavenumber corresponding to the maximum of the energy spectrum $|\eta_\omega|^2$. In all our experiments $k_m$ was approximately the same and located in the forcing range, $k_m \approx 5.7\mathrm{m}^{-1}$ that corresponds to the wavelength $\lambda \approx 1.1$ m. In this experiment the range of the nonlinearity parameter was $0.1 < \gamma < 0.25$.

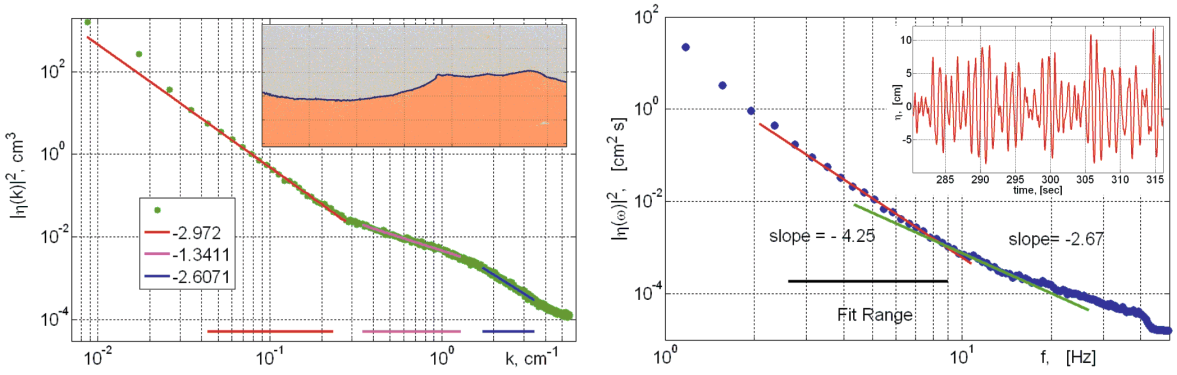


FIG. 5: Left plot: The spectrum in $k$-domain. The inset shows an image of air-water interface. Right plot: The spectrum in $\omega$-domain. The inset shows a correspondent function $\eta(t)$. Both spectra were measured at the wave nonlinearity $\gamma$=0.2.

## IV. RESULTS.

### A. Spectra.

Typical energy spectra in the $\omega$ and $k$ domains are shown in Figures 5. For the $\omega$-spectra we usually have about one decade of the fitting range which, according to the dispersion relation, should correspond to the two decades for the $k$-spectra. In reality the $k$-spectra have shorter scaling range which is limited, on the low $k$-side, by the width of laser sheet,1.2m, and on the high $k$-end by insufficient vertical resolution of the images and limited statistics. In addition, the scaling ranges getting narrower for the flume runs with weaker forcing.

The slopes of the energy spectra in the $\omega$ and $k$-domains as functions of the wave field intensity are shown in Fig. 6. We see that for both $\omega$ and $k$ spectra the slopes are steeper for the weaker wave fields with respect to the stronger ones. One can see that at low wave intensities the data scatter and uncertainty are much greater than for stronger wave turbulence in agreement with the previous measurements of the $\omega$ spectra in [2].

In Figure 7 we show of graph of the $k$-slope versus the $\omega$-slope for the energy spectra measured in the same experiments with the laser sheet and the capacitance wire techniques respectively. The linear dispersion slope is shown by the solid curve. As we see, the experimental data deviate significantly from the linear dispersion curve, which indicates that, at least in the fitting ranges of scales, the nonlinearity is not weak.

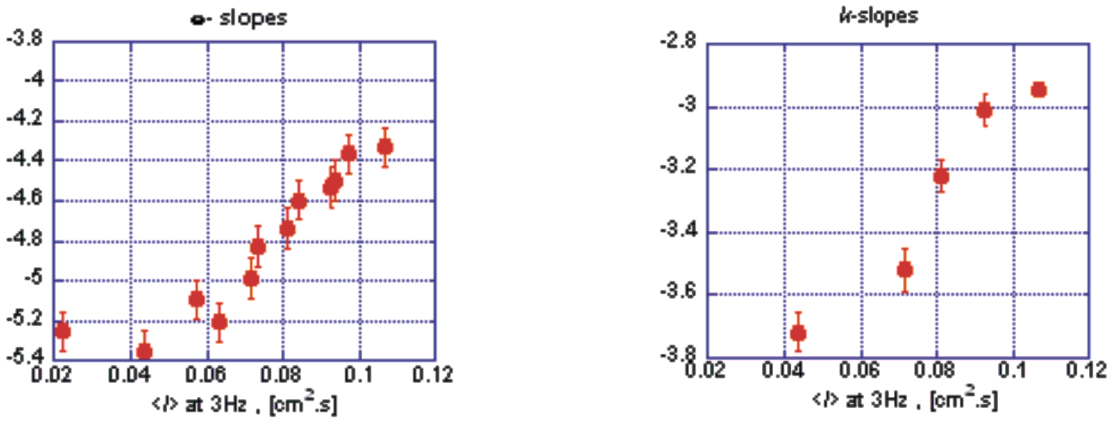


FIG. 6: Slopes of the $k$- and $\omega$-spectra as functions of the wave intensity, $I = |\eta_\omega|^2$, measured at the frequency 3Hz in $\omega$-spectrum.

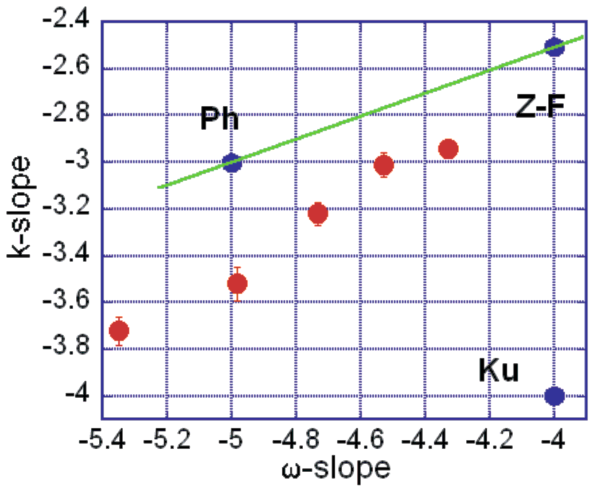


FIG. 7: The $k$-slope vs $\omega$-slope. The linear dispersion relation, $\omega = \sqrt{gk}$, is shown by the solid line. Ph, ZF and Ku mark the points corresponded to Phillips, Zakharov-Filonenko and Kuznetsov predictions respectively.

We also put the points corresponding to the theoretical predictions: Ph, ZF and Ku spectra. We see that both Ph and Ku points are rather far from the experimental data, whereas ZF point is more in agreement with the experiment. Namely, this plot suggests that if one would perform experiments at even higher amplitudes then it is quite likely that the experimental data would have crossed the ZF point. This result is rather surprising because one would naturally expect the ZF theory to work better for weaker rather than for stronger

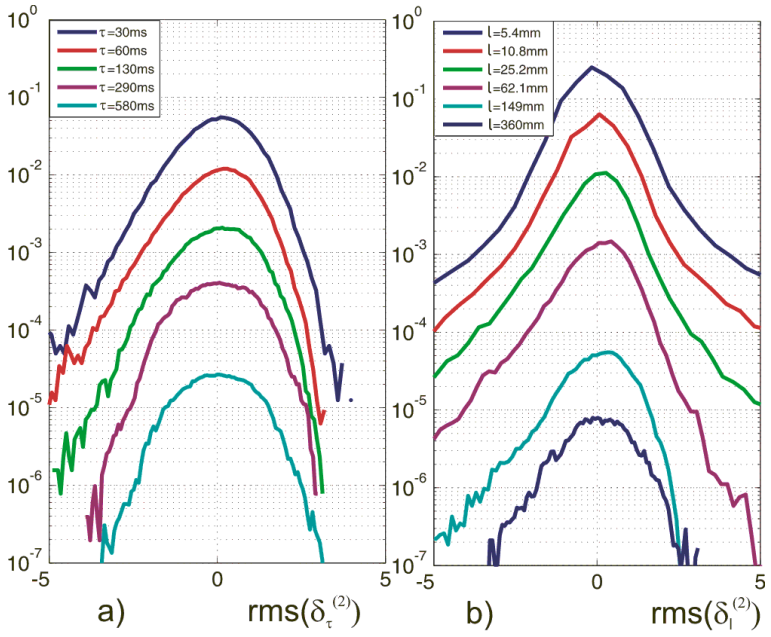


FIG. 8: PDFs of second-order differences: a) in the $t$-domain, b) in the $x$-domain.

waves. However, as we mentioned before, the finite flume size effects are more important for weaker waves, which is the most likely explanation why there is a significant deviation from the ZF spectrum at smaller wave amplitudes. Note that the simultaneous measurement of the $k$ and $\omega$-spectra allows one to resolve the uncertainty of the previous results reporting on the the $\omega$-spectra only. Namely, we are now able to differentiate between the ZF and Ku states which have undistinguishable $\omega$-slopes but different $k$-slopes. The result is that ZF spectrum is more in agreement with the experimental data than the Ku spectrum. However, as we will see, coherent singular structures of the type discussed by the Ku theory do seem to leave their imprints on the scalings of the high order structure functions.

### B. PDFs of the height increments.

To present results on the PDFs and the SFs we select the experimental run with spectra $E_k \sim k^{-3.02}$ and $E_\omega \sim \omega^{-4.53}$. Because for each of these spectra both $k$ and $\omega$ slopes are steeper than -3 but shallower than -5, we choose to work with the second-order increments, $j = 2$. Experimental PDFs of the height increments in space and time are shown in Figs. 8a and 8b respectively. For the space increments, one can see clearly deviations from Gaussianity at the (fat) PDF tails which are related to intermittency and indicate presence of

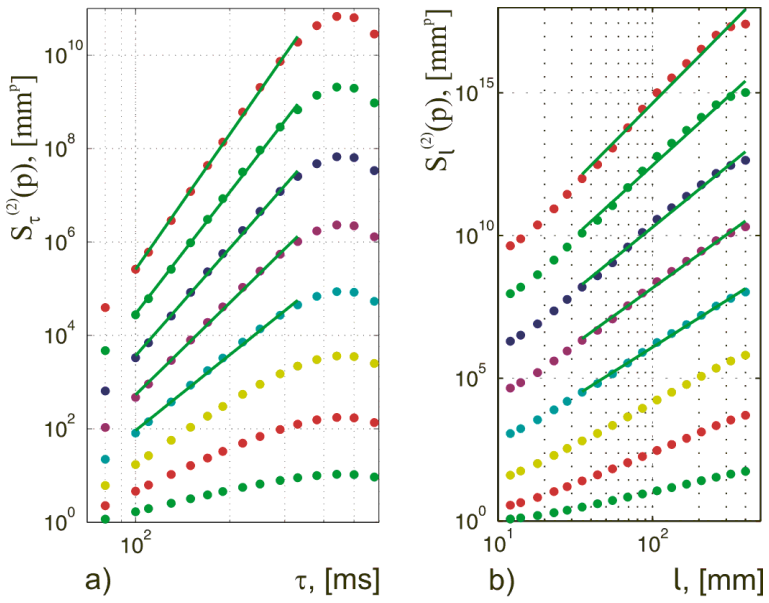


FIG. 9: The elevation structure functions (moments) from the 1st to 8th order (p=1, ... ,8): a) in the $t$-domain, $S_\tau^{(2)}(p)$, and b) in the $x$-domain, $S_l^{(2)}(p)$, as the functions of $\tau$ and $l$ respectively.

the coherent structures. For the time increments, the deviations from Gaussianity is much less pronounced, which could be due to the slow propagation speed of the coherent structures leading to their more infrequent occurrence in the $t$-domain in comparison with the $x$-domain. Both the $t$- and the $x$-domain PDF's are asymmetric (with the negative increments dominant) which results from breaks occurring at wave crests rather than troughs.

### C. Structure functions.

In our data on the SFs, both $S_\tau^{(2)}(p)$ as a function of $\tau$ and $S_l^{(2)}(p)$ as a function of $l$ exhibit clear power-law scalings in the range of scales corresponding to the gravity waves for all $p$ at least up to 8 (see Fig. 9). The SF exponents for the time and space domains are shown in Figs. 10a and 10b respectively. Straight lines on these graphs represent the ZF scaling (solid line, red online), scaling of waves with the spectrum as measured in the experiment (dash line, green online) and the fit of the high-$p$ behavior with a scaling corresponding to singular coherent structures (dash-dot line, blue online). For the time domain, the scaling at low $p$ is close to the ZF scaling, this is surprisingly more consistent than with the scaling calculated from the actual measured spectrum. For an infinite scaling range the $p = 2$ point must, of course, lie exactly on the value corresponding to the spectrum, $(\nu - 1)$, irrespective of the

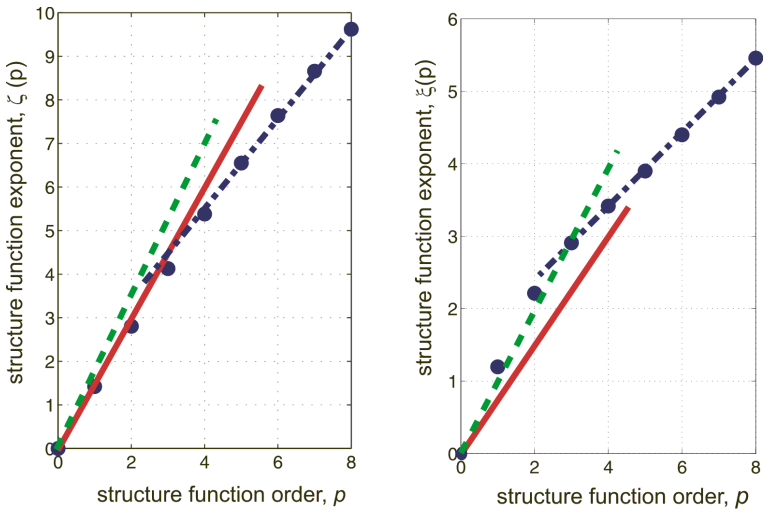


FIG. 10: Structure functions scaling exponents a) $\xi(p)$ in the $k$-domain and b)$\zeta(p)$ in the $t$-domain. Red-solid line represents ZF scaling, green-dash line - the scaling obtained in the experiment, blue-dash-dot line - the scaling for coherent structures.

presence or absence of the phase correlations. Thus we attribute the observed discrepancy to the finiteness of the scaling range. Furthermore, the fit of the high $p$ dependence indicates the presence of singular coherent structures with $D = 1, a = 1.05$ that is very close to the Ku's $D = 1, a = 1$.

For the space-domain, at low $p$ there is an agreement with the scaling of the random phased waves having the actual measured spectrum, and less agreement with the random phased waves having the ZF spectrum. This is not surprising since the scaling range in $k$ is greater than in $\omega$ and therefore there is a better agreement between the spectrum and the SF exponent for $p = 2$. More importantly we see again the dominance of the random phased waves in the low-order SFs, and the dominance of coherent breaks in the high-order SFs. The fit at high $p$'s gives for the dimension and the singularity parameter of the breaks $D = 1.3$ and $a = 1/2$ respectively. We see that the breaks appear to be more singular and "spiky" than the Ku-type breaks (a = 1). Visually, we observed numerous occurrences of these kinds of spiky wave breaks, which are not propagating (or propagating very slowly) and producing vertical splashes. These kinds of structures should be probable in isotropic wave fields due to the collision of counter-propagating waves, which in our flume appear due to multiple wave reflections from the walls. The slow propagation speed of such breaks means their seldom crossing through the capacitance probe even if there is a large number

of them in the $x$-domain (i.e. more than the Ku-type breaks). This could explain why the Ku-breaks show up in the SF scalings in the $t$-domain, whereas more singular spiky structures are seen in the $x$-domain.

### D. Statistics of the Fourier modes.

Let us now present results on the statistics of the Fourier modes. Immediately, we should be cautions about the applying the theory of the Fourier mode statistics and intermittency cycle described above in the theoretical part of the paper. Firstly, the theoretical picture was developed for weak waves where random waves dominate over the coherent structures in most of the inertial range, whereas the experimental runs selected in the present work corresponded to larger excitations where the rms amplitude and wavebreaking amplitude are not different by orders of magnitude. Secondly, like classical WTT, the theory corresponds to an infinite system, whereas the finite size effects are likely to be important in our flume. Recall that the finite size effects are strongest at low amplitudes, and it is impossible to implement weak wave turbulence and eliminate the finite size effects simultaneously in our flume. Thirdly, our statistical data is not sufficient for the single Fourier modes and, as a result, the PDF tails are rather noisy. One can reduce this noise by combining several adjacent Fourier modes, but in doing this one has to be careful not to reduce or eliminate the tail due to such an averaging (i.e. one can only combine modes which are strongly correlated).

Nonetheless, the results on Fourier space PDFs are quite illuminating and worth presenting. PDFs of $\omega$-modes, $J_\omega = |\eta_\omega|^2$, as measured by the wire probes were first presented in [2] and we reproduce them in Figure 11. Here, the averaging was done over modes in the frequency range from 5.5 to 6.5 Hz via bandpass filtering. One can see that the PDF core can be fitted with an exponential function which corresponds to gaussian statistics. At the tail one can see a significant deviation from the exponential fit corresponding to intermittency. As predicted by the theory, the tail follows a power law (with cutoff), but with a different index, $-3$ rather than $-1$. This deviation in the power-law index could be due to one of the reasons mentioned in the beginning of this subsection.

PDFs of $k$-modes, $J_k = |\eta_k|^2$, are shown in Figure 12. Here, the averaging was done over 3 adjacent modes. Again, we see a Gaussian PDF core and a power-law tail, - now with

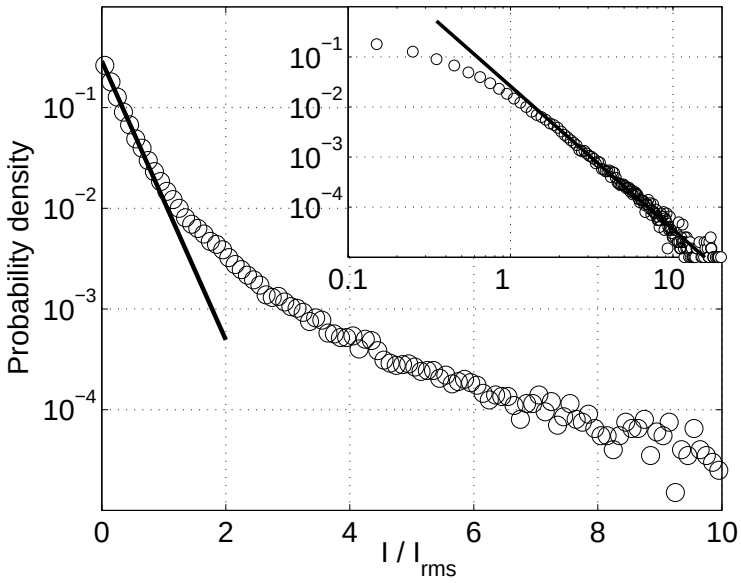


FIG. 11: Normalized PDF of the spectral intensity $I = |\eta_w|^2$ band-pass filtered with the frequency window $\pm 1Hz$ centered at $f$ =6 Hz, measured at wave nonlinearity $\gamma = k_0\eta_{rms} \approx 0.16$ ($k_0$ is the wave vector at the maximum spectral power). The inset shows the same plot in log-log coordinates.

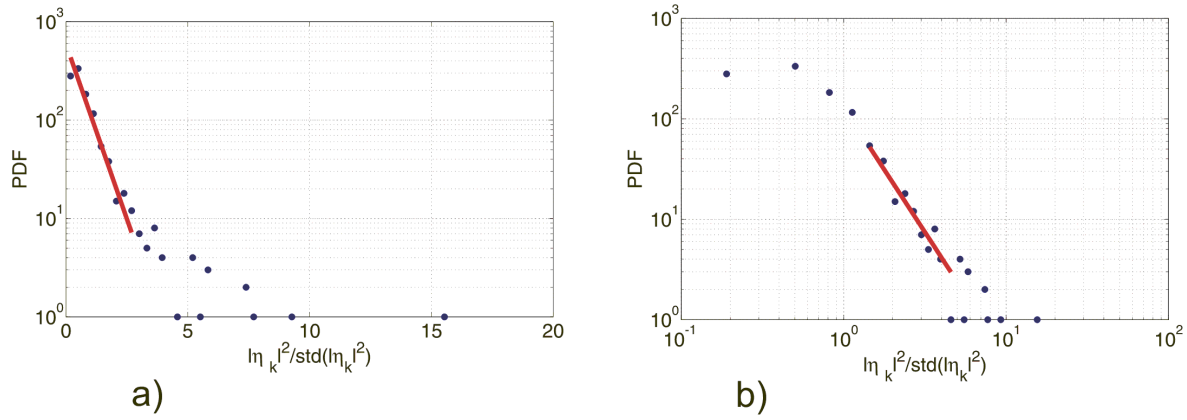


FIG. 12: The PDF of the $k$-mode centered at $k$=54.3rad/m, filtered within the window $\pm$10.8rad/m and normalized by its standard deviation. a)A semilog plot with the exponential fit $y \propto 10^{-1.6x}$ b) A loglog plot with the power fit $y \propto x^{-2.5}$.

index $-2.5$, which also different from the theoretical index $-1$. The fact that the PDF tail for the $k$-modes decays slower than for the $\omega$-modes ($k^{-2.5}$ vs $k^{-3}$) is consistent with our conclusion (which we have made based in the statistics of the $x$ and $t$-domain increments) that turbulence shows stronger intermittency in space than in time.

## V. SUMMARY AND DISCUSSION.

We have presented a theory and performed measurements of gravity wave turbulence statistics in both $x$ and $t$-domains. This allowed us to differentiate between the states which have the same frequency spectra but different $k$-spectra, particularly between the ZF and Ku states. Our data indicate that the spectral exponents, both in $\omega$ and $k$, depend on the amplitude of the forcing. There is a certain evidence favoring ZF theory at larger wave amplitudes, but the ZF state in not possible to observe in its purity because the two fundamental limits of WTT, weak nonlinearity and the infinite box, are impossible to implement simultaneously even in such rather large flume as ours. None of the existing theories, relying on the presence of either random phased weakly nonlinear waves or on dominance of coherent wave crests of a particular type, can fully explain our experimental results. Instead, there is an indication that the gravity wave field consists of coexisting and interacting random and coherent wave components. The random waves are captured by the PDF cores and the low-order SF's, whereas the coherent wave crests leave their imprints on the PDF tails and on the high-order SF's. The singular wave crests themselves consist of structures of different shapes: numerous non-propagating spikes/splashes (which show in the $x$-domain SF's) and propagating Ku-type breaks (seen in the $t$-domain SF's). We suggested a plausible scenario for the dynamics and mutual interactions of these coexisting random-phased and coherent wave components based on a turbulence cycle. Namely, the coherent structures appear in the process of the energy cascade within the random wave component (when the nonlinearity becomes strong at some scale along the cascade). The coherent waves partially dissipate their energy due to wave breaking and partially they return energy to a wide range of longer incoherent waves. Based on this picture, we made qualitative theoretical predictions for the scalings of the moments of the Fourier modes. However, our present statistical data is insufficient for building these moments, and longer experimental runs are needed in future to accumulate this statistics.

## VI. ACKOWLEDGEMENTS.

This work was partially done during the EPSRC sponsored Warwick Turbulence Symposium programme 2005-2007. The authors are grateful to the Hull Environmental Research

Institute for a partial financial support and B. Murphy for his help with experiments at the Deep flume.

---

[1] Peter A.E.M. Janssen, *The Interaction of Ocean Waves and Wind*, Cambridge University Press, 2004.

[2] P. Denissenko, S. Lukaschuk and S. Nazarenko, Gravity wave turbulence in a laboratory flume. Phys. Rev. Lett. **99**, 014501 (2007).

[3] E. Falcon, C. Laroche and S. Fauve, Observation of gravity-capillary wave turbulence. Phys. Rev. Lett. **98**, 094503 (2007).

[4] V.E. Zakharov and N.N. Filonenko, J. Appl. Mech. Tech. Phys. **4** , 506-515 (1967);

[5] V.E. Zakharov, V.S. L'vov and G. Falkovich, *Kolmogorov Spectra of Turbulence*, Springer-Verlag, 1992.

[6] E.A. Kuznetsov, Turbulence spectra generated by singularities. JETP Letters, **80**, 83-89, (2004).

[7] Y. Choi, Y. Lvov, S. Nazarenko and B. Pokorni, Anomalous probability of large amplitudes in wave turbulence. Physics Letters A, **339**, Issue 3-5, 361-369 (2005); (arXiv:math-ph/0404022 v1 Apr 2004).

[8] K. Hasselmann, J. Fluid Mech. **12**, 481 (1962);

[9] S.V. Nazarenko, Sandpile behavior in discrete water-wave turbulence. J. Stat. Mech. L02002 (2006) doi:10.1088/1742-5468/2006/02/L02002 (arXiv:nlin.CD/0510054).

[10] E.A. Kartashova, On properties of weakly nonlinear wave interactions in resonators. Physica D **54**, 125 (1991).

[11] E. Kartashova, Wave resonances in systems with discrete spectra. AMS Transl. (2) **182** (1998).

[12] B.B. Kadomtsev, *Plasma Turbulence*, p. 63, Academic Press, New York, 1965.

[13] O.M. Phillips, The equilibrium range in the spectrum of wind generated waves. J. Fluid Mech. **4**, 426-434 (1958).

[14] C. Connaughton, S. Nazarenko, A.C. Newell, *Dimensional analysis and weak turbulence*, Physica D, **184**, 86-97 (2003);

[15] S. Dyachenko, A.C. Newell, A. Pushkarev, and V.E. Zakharov, Optical turbulence: weak turbulence, condensates and collapsing filaments in the nonlinear schrodinger equation. Physica

**D 57**, 96 (1992).

[16] A.C. Newell, S. Nazarenko and L. Biven, Wave turbulence and intermittency. Physica **D 152-153**, 520 (2001).

[17] A.C. Newell, V.E. Zakharov, The role of the generalized Phillips' spectrum in wave turbulence. Phys. Lett. A**372**, 4230 (2008).

[18] M.A. Mukto, M.A. Atmane, M.R. Loewen, A particle-image based wave profile measurement technique. Exp. Fluids **42**, 131-142 (2007).

[19] V.P. Krasitskii, On reduced equations in the Hamiltonian theory of weakly nonlinear surface-waves. J. Fluid Mech. **272**, 1 (1994).